# Cascaded Entanglement Enhancement

Zhihui Yan, Xiaojun Jia,* Xiaolong Su, Zhiyuan Duan, Changde Xie, and Kunchi Peng
*State Key Laboratory of Quantum Optics and Quantum Optics Devices,*
*Institute of Opto-Electronics, Shanxi University, Taiyuan, 030006, P. R. China*

We present a cascaded system consisting of three non-degenerate optical parametric amplifiers (NOPAs) for the generation and the enhancement of quantum entanglement of continuous variables. The entanglement of optical fields produced by the first NOPA is successively enhanced by the second and the third NOPAs from $-5.3\ dB$ to $-8.1\ dB$ below the quantum noise limit. The dependence of the enhanced entanglement on the physical parameters of the NOPAs and the reachable entanglement limitation for a given cascaded NOPA system are calculated. The calculation results are in good agreement with the experimental measurements.

PACS numbers: 03.67.Bg, 42.50.Dv, 03.65.Ud, 42.50.Lc



Nonlocal quantum entanglement is the key resource to realize quantum information processing (QIP) [1–3]. The entangled states of single photons (qubits) and optical modes (qumodes) have been applied in QIP with discrete and continuous variable (DV and CV) regimes, respectively [4, 5]. The quadrature squeezed states of light are the essential resource states in CV QIP since squeezing is the necessary base to establish quantum entanglement among optical fields [6]. A scheme of generating CV optical entangled states is to interfere two single-mode squeezed states of light with an identical frequency and a constant phase-difference on a $50/50$ beamsplitter [5, 7]. The two single-mode squeezed states are often produced by a pair of degenerate optical parametric amplifiers (DOPAs) with identical type-I nonlinear crystal pumped by a laser to ensure high interference efficiency. Through carefully technical improvement on suppressing the phase fluctuation of optical field and reducing the intra-cavity losses of DOPA, the squeezing level of the single-mode squeezed states is continually renewed in recent years [8–10]. So far, the squeezing over $-12\ dB$ below the quantum noise limitation (QNL) has been achieved by a group in Hannover [9, 10]. Coupling a single-mode squeezed state of $-9.9\ dB$ and a vacuum field on a $50/50$ beam splitter, the Einstein-Podolsky-Rosen (EPR) entangled state of light (also named two-mode squeezed state) with the quantum correlation of amplitude and phase quadratures of $-3\ dB$ below the QNL was obtained in 2011 [11]. The four-mode CV entanglement of $-6\ dB$ below the QNL was achieved by combing four initial single-mode squeezed states generated by four DOPAs [12]. The highest CV entanglement produced by coupling single-mode squeezed states is $-6\ dB$ below the QNL up to now [12].

Another important device to generate CV EPR entangled state of optical field is the non-degenerate optical parametric amplifier (NOPA) consisting an optical cavity and a type-II nonlinear crystal. Through the intra-cavity frequency-down conversion process in a NOPA, a pair of non-degenerate optical modes with amplitude and phase quadrature correlations is directly produced, which is an EPR entangled state [13]. Twenty years ago, Kimble's group experimentally generated a pair of CV entangled optical beams with a NOPA and demonstrated the EPR paradox firstly in CV regime [13]. Then, NOPAs operating at different version (above or lower the threshold, amplification or de-amplification) are used as the sources of generating optical CV entangled states and the produced EPR beams are applied in a variety of CV QIP experiments [14–19]. However, in a long period the EPR entanglement level was kept around $-4\ dB$ or lower [13–19]. Until 2010, after a series of strictly technical improvement on the NOPA system, the EPR entanglement degree was raised to $-6\ dB$ [20], which is the best reported result on NOPA system.

In order to obtain high levels of squeezing and entanglement using a single DOPA or NOPA, the device has to be optimized to achieve low phase fluctuations and low optical losses. Especially, a nonlinear optical crystal with a high second-order nonlinear coefficient and low loss is desired. However, the quality of nonlinear crystals and optical elements is not ideal usually. In the quantum manipulation experiments of CV entangled states, we found that the EPR entanglement of optical field produced by an NOPA can be enhanced by another NOPA under appropriate operation condition [21, 22]. The amount of the enhanced entanglement is limited by the physical parameters of the used NOPA. For further raising entanglement under generally technical condition, we design the cascaded NOPA system involving three NOPAs and experimentally realized the cascaded amplification of CV entanglement. The initial EPR entanglement of $-5.3\ dB$ produced by the first NOPA (NOPA1) is enhanced to $-7.2\ dB$ by the second one (NOPA2) and successively to $-8.1\ dB$ by the third one (NOPA3), which is the highest EPR entanglement of optical modes obtained by experiments so far to the best of our knowledges. We numerically calculate the correlation variances of the enhanced EPR entangled state based on the physical parameters of the experimental system. The calculated results are in good agreement with the experimental measurements.

Fig.1 shows the principle schematic of the cascaded entanglement enhancement system. The laser source is an intra-cavity frequency-doubled CW laser, the output second-harmonic wave ($\omega_p$) from which is used for the pump fields of the three NOPAs and the output fundamental wave ($\omega_{p/2}$) serves as the injected signal of NOPA1 and the local oscillator (LO) of the balanced homodyne detector (BHD) for the entanglement measurement. The EPR entangled light generated by

* jiaxj@sxu.edu.cn

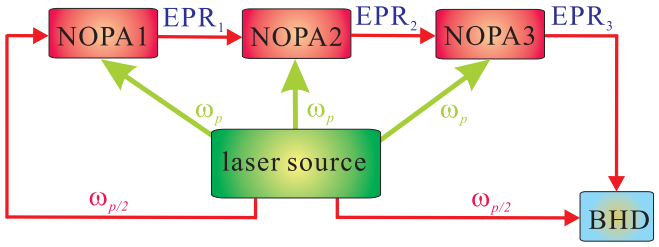


FIG. 1. (Color online) The principle schematic of the cascaded entanglement enhancement system.

NOPA1 (EPR1) is injected into NOPA2 as the injected signal for the first-stage enhancement of the entanglement and the the amplified EPR optical field (EPR2) is injected into NOPA3 for the second-stage enhancement. The final entangled light (EPR3) is detected by the BHD. To achieve the optimal entanglement enhancement, the three NOPAs should be operated at an identical state [21, 22]. In the presented experiment, the three NOPAs are operated below the oscillation threshold of NOPA and at the de-amplification state, i.e. the pump field and the injected signal are out of phase (with the phase difference of $(2n+1)\pi$, $n$-integer). We also require that the signal and idler modes obtained through the frequency-down-conversion of the pump field inside the NOPA have an identical frequency ($\omega_{p/2}$) and the orthogonal polarization, which is easily satisfied in experiments [13–16]. In this case the produced entangled states have the correlated amplitude-sum and phase-difference as well as the anti-correlated amplitude-difference and phase-sum [14–16].

In the following we calculate the correlation variances between the amplitude and phase quadratures of the EPR entangled state enhanced by a NOPA firstly. We describe the quantum state of light with the electromagnetic field annihilation operators $\hat{a} = (\hat{X} + i\hat{Y})/2$, where $\hat{X}$ and $\hat{Y}$ are the operators of the amplitude ($\hat{X}$) and the phase ($\hat{Y}$) quadratures, respectively. $\hat{X}$ and $\hat{Y}$ satisfy the canonical commutation relation $[\hat{X}, \hat{Y}] = 2i$. For generating high EPR entanglement in experiments, the operation conditions of the sub-harmonic signal ($\hat{a}_1$) and idler ($\hat{a}_2$) modes in NOPA should be balanced, i. e. they have the same transmissivity efficiency ($\gamma_1$) on the input-output coupler of the optical cavity (Supposing that a cavity mirror serves as the input and the output coupler simultaneously. See Fig. 3) and the identical intra-cavity loss ($\gamma_2$). The correlation variances and the anti-correlation variances of the injected EPR optical modes, which is produced by the former NOPA, are expressed by $\langle\delta^2(\hat{X}^{in}_{a_1}+\hat{X}^{in}_{a_2})\rangle = \langle\delta^2(\hat{Y}^{in}_{a_1}-\hat{Y}^{in}_{a_2})\rangle = 2e^{-2r}$ and $\langle\delta^2(\hat{X}^{in}_{a_1}-\hat{X}^{in}_{a_2})\rangle = \langle\delta^2(\hat{Y}^{in}_{a_1}+\hat{Y}^{in}_{a_2})\rangle = 2e^{2r+2r'}$, where $r$ and $r'$ are the correlation parameter and the extra noise factor on the anti-correlation components, respectively; $\hat{X}^{in}_{a_{1(2)}}$ and $\hat{Y}^{in}_{a_{1(2)}}$ stand for the amplitude and the phase quadratures of the injected mode $\hat{a}^{in}_{1(2)}$, respectively [21, 23]. Solving the quantum Langevin motion equations and using the input-output relation of the NOPA, the correlation variances of the output field are obtained:

$$
\begin{aligned}
&\langle\delta^2(\hat{X}^{out}_{a_1}+\hat{X}^{out}_{a_2})\rangle = \langle\delta^2(\hat{Y}^{out}_{a_1}-\hat{Y}^{out}_{a_2})\rangle \\
&= (\zeta(2\frac{(-\kappa+\gamma_1-\gamma_2)^2+(\omega\tau)^2}{(\kappa+\gamma_1+\gamma_2)^2+(\omega\tau)^2}e^{-2r} \\
&\quad +2\frac{(2\sqrt{\gamma_1\gamma_2})^2}{(\kappa+\gamma_1+\gamma_2)^2+(\omega\tau)^2}) + 1 - \zeta)\cos^2\theta \\
&\quad +(\zeta(2\frac{(-\kappa+\gamma_1-\gamma_2)^2-(\omega\tau)^2}{(\kappa+\gamma_1+\gamma_2)^2+(\omega\tau)^2}e^{2r+2r'} \\
&\quad +2\frac{(2\sqrt{\gamma_1\gamma_2})^2}{(\kappa+\gamma_1+\gamma_2)^2+(\omega\tau)^2}) + 1 - \zeta)\sin^2\theta, \qquad (1)
\end{aligned}
$$

where $\hat{X}^{out}_{a_{1(2)}}$ and $\hat{Y}^{out}_{a_{1(2)}}$ are the amplitude and the phase quadratures of the output mode $\hat{a}^{out}_{1(2)}$, respectively; $\kappa = \beta\chi$ is the nonlinear coupling efficiency of the NOPA which is proportional to the pump parameter $\beta = (p_{pump}/p_{th})^{1/2}$ ($p_{pump}$ - the pump power, $p_{th}$ - the threshold pump power of NOPA) and the second-order nonlinear coupling coefficient $\chi$ of the nonlinear crystal used in the NOPA; $\tau$ is the round-trip time of light in the optical cavity; $\omega = 2\pi\Omega$ is the noise analysis frequency; $\zeta$ is the imperfect detection efficiency; and $\theta$ is the relative phase fluctuation between the pump field and the injected signal resulting from imperfect phase-locking.

Fig. 2 (a) is the calculated dependence of correlation variances of the output EPR optical field from NOPA3 on

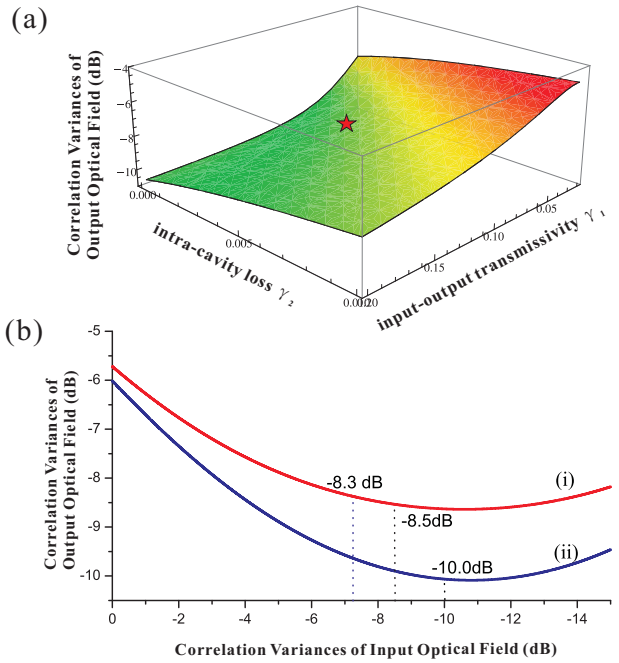


FIG. 2. (Color online) (a) The dependence of correlation variances of the output entangled optical field on the input-output transmissivity $\gamma_1$ and the intra-cavity loss $\gamma_2$ of NOPA. (b) The functions of the correlation variances of the output field vs that of the input field for two NOPAs: (i) $\gamma_1 = 0.1$, $\gamma_2 = 0.004$; (ii) $\gamma_1 = 0.1$, $\gamma_2 = 0.001$.

the cavity parameter $\gamma_1$ and $\gamma_2$, where other parameters are taken according to the really experimental system ($r = 0.83$; $r' = 0.45$; which correspond to the entanglement degree of EPR2 with correlation variance of -7.2 dB below the QNL and the anti-correlation variance of 11.1 dB above the QNL, see the experimental results in the text; $\theta = 0.0105; \Omega = 2.0\ MHz; \tau = 2.0 * 10^{-9}\ s; \varsigma = 0.947$.). When $\gamma_1$ increases and $\gamma_2$ decreases the correlation variance of the output field reduces, i.e. the entanglement degree increases. It means that for a simple NOPA the higher input-output transmissivity ($\gamma_1$) and the lower intra-cavity loss ($\gamma_2$) can provide the stronger performance of the entanglement enhancement. However, for a NOPA with given physical parameters, the correlation variances of the output field depend on the correlation variances of the injected signal field. Fig. 2 (b) shows the functions of the correlation variances of the output field vs that of the input field, where the trace (i) for $\gamma_1 = 0.1$, $\gamma_2 = 0.004$ and the trace (ii) for $\gamma_1 = 0.1$, $\gamma_2 = 0.001$; other parameters are the same as that of Fig. 2 (a). We can see from Fig. 2 (b), there is a turning point in the trace (i) ($-8.5\ dB$) and (ii) ($-10.0dB$), respectively, where the correlation variance of the output field equals to that of the input field. And after the turning point the correlation variances of the output field will be larger than that of the input signal. It means the enhancement ability of the NOPA no longer exists. Comparing traces (i) and (ii), it is obvious that the NOPA with the smaller intra-cavity loss (trace (ii)) has stronger ability of the entanglement enhancement. For a given NOPA, the ability of the entanglement enhancement decreases when the entanglement of the injected field increases. After the turning point of the trace (i) and (ii), the entanglement of the output field becomes worse than that of the input field, i.e. there is an upper limitation of the entanglement of the input field for a given NOPA. When the entanglement of the input field surpasses the limitation value, the entanglement of the output field starts to reduce. This is because the noises of the anti-correlation components in the input field increase rapidly along with the increasing of the correlation degree, and the noises on the anti-correlation components would be inevitably coupled to the correlation component and thus decrease the correlation degree of the output fields due to the existence of the phase fluctuation $\theta$ in the experimental system (See the second term of Eq. (1)). Reducing the phase fluctuation in the phase-locking system, the upper limitation of the input field for the entanglement enhancement will be raised.

The experimental setup is shown in Fig.3. A continuous-wave intra-cavity frequency-doubled and frequency-stabilized Nd:YAP/LBO (Nd-dropped $YAlO_3$/$LiB_3O_5$) laser (Yuguang Co. Ltd., FG-VIB) with both the harmonic-wave output at $540\ nm$ and the subharmonic-wave output at $1080\ nm$ serves as the laser source of the entanglement enhancement system. The output green and infrared lasers are separated by a beam splitter M10 coated with high reflection for $540\ nm$ and high transmission for $1080\ nm$. The green laser serves as the pump fields of three NOPAs and the infrared laser is used for the injected signal of NOPA, as well as the local oscillators (LO) of BHD1 and BHD2. The traveling-wave mode cleaners (MC1 for $540\ nm$ and MC2 for $1080\ nm$) consisting of three mirrors are used for the optical low-pass filters of noises and the spatial mode cleaners. The finesses of MC1 for $540\ nm$ and MC2 for $1080\ nm$ both are 550. The optical isolators (ISO1 for $540\ nm$ and ISO2 for $1080\ nm$) are utilized to prevent the feedback optical fields from the NOPA returning to the laser. We choose the $\alpha$-cut Type II KTP ($KTiOPO_4$) to be the nonlinear mediums in the three NOPAs, which can achieve type-II noncritical phase-matched frequency-down-conversion of the pump field at 1080 nm. The size of the three KTP crystals is the same ($3 * 3 * 10mm^3$) and temperature of the KTP crystal in the three NOPAs is controlled around $63°C$ to satisfy the phase-matching condition. Since the phase-matching temperature of KTP has a broad full width of about $30°C$, we can make the signal and the idler modes double-resonating inside a NOPA by carefully tuning the temperature of the crystal around $63°C$. The NOPA1 is in a semi-monolithic Fabry-Perot configuration consisting of a KTP crystal and a concave mirror (M1) with $50\ mm$ radius of curvature. The front face of the crystal is coated to be used as the input coupler of the pump field (the transmissivity of $99.8\%$ at $540\ nm$ and $0.04\%$ at $1080\ nm$), and the other face is coated with the dual-band antireflection at both $540\ nm$ and $1080\ nm$. M1 coated with transmissivity of $5.2\%$ at $1080\ nm$ and high reflection at $540\ nm$ is used as the output coupler and is mounted on a piezoelectric transducer (PZT1) to scan actively the cavity length of NOPA1 or lock it on resonance with the injected signal as needed. The length and the finesse of the cavity of NOPA1 are $54\ mm$ and 115, respectively. The NOPA2 (3) has the ring configuration consisting of two flat mirrors M2 (6) and M3 (7) and two concave mirrors M4 (8) and M5 (9) with $100\ mm$ radius of curvature. The KTP crystal with the $1080\ nm$

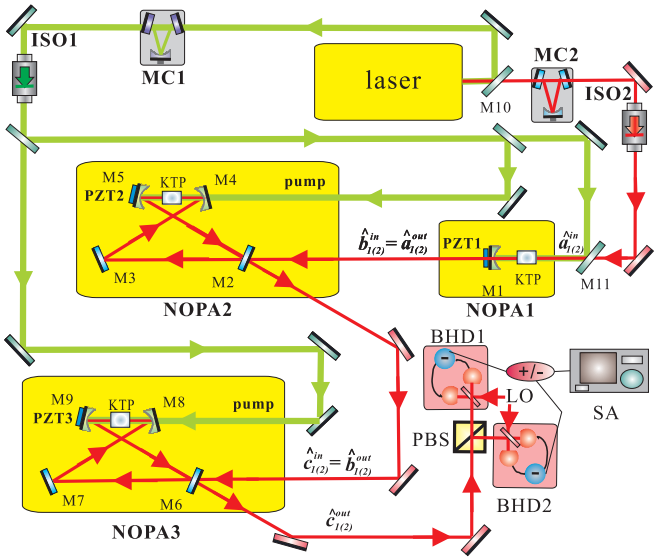


FIG. 3. (Color online) The experimental setup of cascade sensitive-phase entanglement enhancement. laser, Nd:YAP/LBO laser source; PBS, polarizing beam splitter; MC1(2), mode cleaner; ISO1(2), optical isolator; M0–M11, different mirrors (see text for details); PZT, piezoelectric transducer; +/-, positive/negative power combiner; SA, spectrum analyzer.

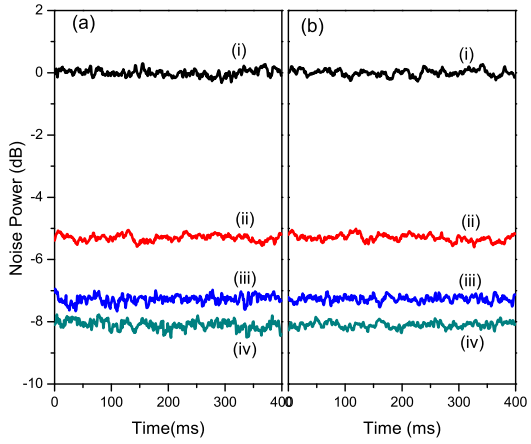


FIG. 4. (Color online) Noise powers of the correlation variances: (a) Trace (i), the QNL; trace (ii), correlation variance of $\langle\delta^2(\hat{X}^{out}_{a_1}+\hat{X}^{out}_{a_2})\rangle$; trace (iii), correlation variance of $\langle\delta^2(\hat{X}^{out}_{b_1}+\hat{X}^{out}_{b_2})\rangle$; trace (iv), correlation variance of $\langle\delta^2(\hat{X}^{out}_{c_1}+\hat{X}^{out}_{c_2})\rangle$. (b) Trace (i), The QNL; trace (ii), correlation variance of $\langle\delta^2(\hat{Y}^{out}_{a_1}-\hat{Y}^{out}_{a_2})\rangle$; trace (iii), correlation variance of $\langle\delta^2(\hat{Y}^{out}_{b_1}-\hat{Y}^{out}_{b_2})\rangle$; trace (iv), correlation variance of $\langle\delta^2(\hat{Y}^{out}_{c_1}-\hat{Y}^{out}_{c_2})\rangle$.

and $540\ nm$ dual-band antireflection coated at both end faces is placed in the middle of M4 (8) and M5 (9). M2 (6) serves as the input-output coupler with the transmission of $10.0\%$ at $1080\ nm$ and antireflection at $540\ nm$, respectively. All the other mirrors are high reflection at $1080\ nm$ and antireflection at $540\ nm$. M5 (9) are mounted on PZT2 (3) for scanning or locking actively the length of the optical cavity NOPA2 (3). The length and the finesse of the cavity for both NOPA2 and NOPA3 are $557\ mm$ and 60, respectively. The threshold pump powers of the three NOPAs are $250\ mW$ for NOPA1 and $900\ mW$ for NOPA2 and NOPA3, respectively. The signal and the idler optical beams with orthogonal polarizations produced by NOPA3 are separated by a polarizing-beam-splitter (PBS) and then are detected by BHD1 and BHD2, respectively. The BHD consists of a $50/50$ beam-splitter and a pair of photodiodes (ETX-500 InGaAs). Locking the relative phase between the signal (idler) beam and the LO to 0 or $\pi/2$, the fluctuations of amplitude or phase quadrature of the signal (idler) field can be measured by BHD1 (BHD2). The noise powers of the amplitude (phase) quadratures simultaneously measured by BHD1 and BHD2 are combined by the positive (negative) power combiner ($\oplus(\ominus)$) and then the correlation variances of the amplitude-sum (phase-difference) are analyzed by a spectrum analyzer (SA).

Figs. 4 (a) and (b) show the measured correlation variances of the amplitude-sum and the phase-difference, respectively. In Fig. 4 (a) [(b)] trace (i) is the QNL, trace (ii), (iii) and (iv) are the measured noise power spectra of the amplitude-sum (phase-difference) at 2 MHz for EPR1, EPR2 and EPR3, respectively. The initial correlation variances of EPR1 produced by NOPA1 are $\langle\delta^2(\hat{X}^{out}_{a_1}+\hat{X}^{out}_{a_2})\rangle = \langle\delta^2(\hat{Y}^{out}_{a_1}-\hat{Y}^{out}_{a_2})\rangle = 0.59$, corresponding to $-5.3\pm0.2\ dB$ below the QNL. After the first-stage enhancement by NOPA2 the correlation variances are reduced to $\langle\delta^2(\hat{X}^{out}_{b_1}+\hat{X}^{out}_{b_2})\rangle = \langle\delta^2(\hat{Y}^{out}_{b_1}-\hat{Y}^{out}_{b_2})\rangle = 0.38$, corresponding to $-7.2\pm0.2\ dB$ below the QNL. At last, after the cascaded enhancement by NOPA2 and NOPA3, the correlation variances of EPR3 become $\langle\delta^2(\hat{X}^{out}_{c_1}+\hat{X}^{out}_{c_2})\rangle = \langle\delta^2(\hat{Y}^{out}_{c_1}-\hat{Y}^{out}_{c_2})\rangle = 0.31$, corresponding to $-8.1\pm0.2\ dB$ below the QNL. The correlation variance of EPR3 is denoted in Fig. 2 (a) with a red star, where $\gamma_1 = 0.1$, $\gamma_2 = 0.004$, $r = 0.83$, ($-7.2\ dB$ below the QNL) corresponding to the operation conditions of NOPA3. On the trace (i) of Fig. 2 (b) we can see, when the correlation variance of the input EPR beam (EPR2) equals to $-7.2\ dB$, the correlation variance of the output field (EPR3) is $-8.3\ dB$ which is in good agreement with the experimental measured value ($-8.1\ dB$). We also measured the anti-correlation variances of EPR1, EPR2 and EPR3, which are $\langle\delta^2(\hat{X}^{out}_{a_1}-\hat{X}^{out}_{a_2})\rangle = \langle\delta^2(\hat{Y}^{out}_{a_1}+\hat{Y}^{out}_{a_2})\rangle = 13.6$, $\langle\delta^2(\hat{X}^{out}_{b_1}-\hat{X}^{out}_{b_2})\rangle = \langle\delta^2(\hat{Y}^{out}_{b_1}+\hat{Y}^{out}_{b_2})\rangle = 25.9$, and $\langle\delta^2(\hat{X}^{out}_{c_1}-\hat{X}^{out}_{c_2})\rangle = \langle\delta^2(\hat{Y}^{out}_{c_1}+\hat{Y}^{out}_{c_2})\rangle = 34.2$ corresponding to $8.3\ dB$, $11.1\ dB$ and $12.3\ dB$ above the QNL, respectively. The sums of the amplitude and the phase correlation variances for EPR1, EPR2 and EPR3 are $1.18$, $0.76$, and $0.62$, respectively, all of which satisfy the inseparability criterion, i.e. these values are smaller than $4$ (when the sum is larger than 4 the signal and the idler optical modes in the output field are separable and thus do not form an entangled state [24, 25]. )

In conclusion, we have experimentally demonstrated that the CV entanglement of optical field can be enhanced by the cascaded NOPA. The upper limitation of the enhanced entanglement depends on the intra-cavity loss ($\gamma_2$) of the NOPA and the relative phase fluctuation $\theta$ of the phase locking system. In our system $\gamma_2 = 0.4\%$ for NOPA3, if $\gamma_2$ can be reduced to $0.1\%$ as that reached by Ref. [10], the entanglement of EPR3 will increase to $-9.6\ dB$ below the QNL. The presented scheme opens an avenue to enhance CV entanglement using easily reachable optical devices.

This research was supported by National Basic Research Program of China (Grant No. 2010CB923103), Natural Science Foundation of China (Grants Nos. 60736040, 11074157 and 60821004), the TYAL.

[1] A. Galindo, and M. A. Martin-Delgado, Rev. Mod. Phys. **74**, 347 (2002).

[2] S. L. Braunstein, and P. van Loock, Rev. Mod. Phys. **77**, 513 (2005).

[3] M. D. Reid et al., Rev. Mod. Phys. **81**, 1727 (2009).
[4] D. Bouwmeester et al., Nature (London) **390**, 575 (1997).
[5] A. Furusawa et al., Science **282**, 706709 (1998).
[6] L. A. Wu, H. J. Kimble, J. L. Hall, and H. Wu, Phys. Rev. Lett. **57**, 2520 (1986).
[7] A. M. Lance, T. Symul, W. P. Bowen, B. C. Sanders, and P. K. Lam , Phys. Rev. Lett. **92**, 177903 (2004).
[8] Y. Takeno, M. Yukawa, H. Yonezawa, and A. Furusawa, Opt. Express, **15**, 4321 (2007).
[9] T. Eberle et al., Phys. Rev. Lett. **104**, 251102 (2010).
[10] M. Mehmet et al., e-print arXiv:1110.3737.
[11] T. Eberle et al., Phys. Rev. A **83**, 052329 (2011).
[12] M. Yukawa, R. Ukai, P. van Loock, and A. Furusawa, Phys. Rev. A **78**, 012301 (2008).
[13] Z. Y. Ou, S. F. Pereira, H. J. Kimble, and K. C. Peng, Phys. Rev. Lett. **68**, 3663 (1992).
[14] X. Y. Li et al., Phys. Rev. Lett. **88**, 047904 (2002).
[15] X. J. Jia et al., Phys. Rev. Lett. **93**, 250503 (2004).
[16] J. Laurat, T. Coudreau, G. Keller, N. Treps, and C. Fabre , Phys. Rev. A **71**, 022313 (2005).
[17] A. S. Villar, L. S. Cruz, K. N. Cassemiro, M. Martinelli, and P. Nussenzveig, Phys. Rev. Lett. **95**, 243603 (2005).
[18] J. T. Jing, S. Feng, R. Bloomer, and O. Pfister, Phys. Rev. A **74**, 041804 (2006).
[19] G. Keller et al., Opt. Express **16**, 9351 (2008).
[20] Y. Wang et al., Opt. Express **18**, 6149 (2010).
[21] H. X. Chen, and J. Zhang, Phys. Rev. A **79**, 063826 (2009).
[22] Y. N. Shang, X. J. Jia, Y. M. Shen, C. D. Xie, and K. C. Peng, Opt. Lett. **35**, 853 (2010).
[23] J. Zhang, C. D. Xie and K. C. Peng, Phys. Lett. A **299**, 427 (2002).
[24] L. M. Duan, G. Giedke, J. I. Cirac, and P. Zoller, Phys. Rev. Lett. **84**, 2722 (2000).
[25] R. Simon, Phys. Rev. Lett. **84**, 2726 (2000).